

# INTERGRANULAR FRACTURE AT ELEVATED TEMPERATURE\*

RISHI RAJ† and M. F. ASHBY‡

The kinetic problem of intergranular fracture at elevated temperatures by the nucleation and growth of voids in the grain boundary is analysed in detail. Diffusional transport accounts for the void growth-rate in the analysis, and the nucleation-rate is obtained by using the concepts of classical nucleation theory. The two are compounded to calculate the time-to-fracture. The influence of grain size, strain-rate, temperature, second phase particles and interface energies is taken into account. Particular attention is given to the presence of inclusions in the boundary; the role of the stress concentration at the interface between the inclusion and the matrix, and the energy of this interface is investigated.

## RUPTURE INTERGRANULAIRE AUX TEMPERATURES ELEVEES

On analyse en détail le problème cinétique de la rupture intergranulaire aux températures élevées par la germination et la croissance de cavités aux joints de grains. Dans cette analyse, le transport de matière par diffusion rend compte de la vitesse de croissance des cavités, et l'on obtient la vitesse de germination en utilisant les concepts de la théorie classique de la germination. On combine croissance et germination pour calculer le temps jusqu'à rupture. On tient compte de l'influence de la taille des grains, de la vitesse de déformation, de la température, de particules d'une seconde phase et des énergies d'interface. On insiste en particulier sur la présence d'inclusions dans les joints. On étudie le rôle de la concentration de contraintes à l'interface inclusion-matrice, et de l'énergie de cet interface.

## INTERGRANULARER BRUCH BEI HÖHEREN TEMPERATUREN

Das Kinetikproblem des intergranularen Bruchs bei höheren Temperaturen durch Keimbildung und Wachstum von Hohlräumen in der Korngrenze wird ausführlich untersucht. Die Analyse zeigt, daß Diffusionstransport zum Wachstum der Hohlräume führt und daß die Keimbildungsgeschwindigkeit mit dem Konzept der klassischen Keimbildungstheorie gewonnen werden kann. Aus beiden wird die Zeit bis zum Bruch berechnet. Der Einfluß von Korngröße, Abgleitgeschwindigkeit, Temperatur, Teilchen der zweiten Phase und Grenzflächenenergien wird berücksichtigt. Insbesondere wird die Gegenwart von Einschlüssen in der Korngrenze betrachtet. Die Rolle der Spannungskonzentration an der Grenzfläche zwischen Einfluß und Matrix und die Energie dieser Grenzfläche werden untersucht.

## 1. INTRODUCTION

Fracture of polycrystalline solids under creep conditions can be caused by the growth and coalescence of voids on the grain boundaries. Under the right conditions, the voids grow by the diffusive motion of vacancies to them.<sup>(1)</sup> The same fracture mechanism has been held responsible for the minimum in time-to-fracture, or in the ductility, sometimes observed when polycrystals are pulled in tension at a constant rate.<sup>(2,3)</sup> The diffusional growth of voids has been analysed by Speight and Harris<sup>(4)</sup> and earlier by Hull and Rimmer,<sup>(5)</sup> and is (at least partly) explained. Their nucleation, on the other hand, is still not completely understood: measurements of their nucleation-rate, for instance, are inconclusive.<sup>(1,6)</sup> It has been suggested that stress concentrations at inclusions and triple points can lead to void nucleation.<sup>(7)</sup>

An analysis is presented here which envelopes many of the aspects of intergranular fracture mentioned above and which can be used to calculate the time to fracture for a given grain size, strain-rate, temperature, size and density of second phase particles in the boundary, and the various interface energies. It uses a unified approach whereby different void configurations (at

least five are possible) can be dealt with simultaneously. We first calculate the time-to-fracture when a fixed number of pre-existing voids is present. Next we apply classical nucleation theory to the nucleation-rate of the voids on non-sliding boundaries and on boundaries which slide. The growth-rate and the nucleation-rate are then compounded, using a numerical method, to calculate the time-to-fracture.

Sliding at a grain boundary which contains inclusions can concentrate the tensile stress at the interface at which the inclusion and the matrix meet. We calculate this interface stress (using an upper bound criterion) and the new nucleation rate and time-to-fracture. The combination of the stress concentration and the high interface energy at an inclusion makes it a probable site for void nucleation. The calculations lead to the conclusion that inclusions should be largely responsible for intergranular fracture at elevated temperatures in polycrystals, and predict the influence of grain size, inclusion size and density, and strain-rate on the ductility of polycrystals.

The notation used in this paper is summarized in Table 1.

## 2. VOID GEOMETRIES

Voids formed at the grain boundaries can have different shapes depending on whether they are formed at two-grain junctions, three-grain junctions, four-grain junctions or at the interface of inclusions present in

\* Received September 13, 1974; revised December 20, 1974.

† Assistant Professor, Department of Mechanical Engineering, University of Colorado, Boulder, Colorado 80302, U.S.A.

‡ University Engineering Department, Trumpington Street, Cambridge CB2 1PZ, England.

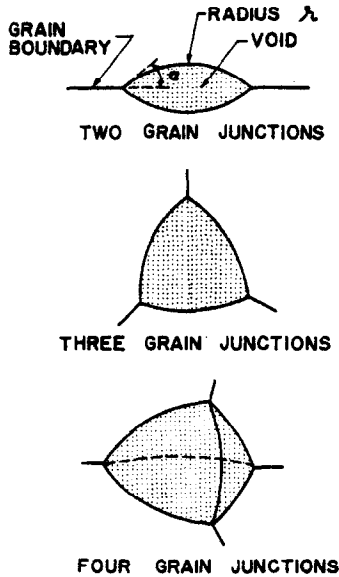


FIG. 1. Void geometries in inclusion free grain boundaries.

the grain boundaries. All voids, however, have two features in common: the free surfaces of the voids are spherical segments (provided that surface diffusion is rapid enough to maintain the uniform curvature† as the void grows) and the angles formed between the void and the interfaces which contain it must be such as to satisfy equilibrium between the surface tension forces in question. The voids considered in this paper fall into two categories: voids formed in inclusion-free grain boundaries; and voids formed in boundaries which contain inclusions.

### 2.1 Voids in inclusion-free boundaries

Figure 1 shows the shapes of voids at two-grain junctions, three-grain junctions and four-grain junctions. The geometry of these voids is described by the radius of the void surface,  $r$ , and the angle  $\alpha$  formed at the junction of the void and the grain boundary. This angle is dictated by equilibrium between surface tension forces at the junction, so that:

$$\alpha = \cos^{-1} \left( \frac{\gamma_B}{2\gamma} \right) \quad (1)$$

where  $\gamma_B$  is the energy (per unit area) of the grain boundary and  $\gamma$  is the energy of the free surface of the void. (Typically for clean surfaces in pure metals,  $\gamma_B \approx \gamma/2$  and  $\alpha \approx 75^\circ$ .)

† This is not always true. Under conditions that cause a void to grow rapidly, matter is removed from its periphery by grain boundary diffusion faster than surface diffusion can redistribute matter on the void surface. It will then become increasingly penny-shaped, and spread in the boundary plane faster than calculated here. For simplicity we neglect this effect.

Three geometric properties of the void—its volume  $V$ , its free surface area  $S$  and the grain boundary area  $B$  that it replaces—can be expressed as functions of  $r$  and  $\alpha$ . In general:

$$V = r^3 F_V(\alpha) \quad (2a)$$

$$S = r^2 F_S(\alpha) \quad (2b)$$

$$B = r^2 F_B(\alpha). \quad (2c)$$

The functions of  $\alpha$  depend on the void type. They have been calculated<sup>(8)</sup> and are quoted in Appendix I for three- and four-grain junctions. For two-grain junctions they are:

$$F_V(\alpha) = \frac{2\pi}{3} (2 - 3 \cos \alpha + \cos^3 \alpha) \quad (3a)$$

$$F_S(\alpha) = 4\pi(1 - \cos \alpha) \quad (3b)$$

$$F_B(\alpha) = \pi \sin^2 \alpha. \quad (3c)$$

Note that as  $\alpha$  increases to  $\pi/2$ , equations (2 and 3) give the properties of a sphere. Remembering that the radius of the circle of intersection of the void with the boundary is  $r_B = r \sin \alpha$  it can be seen that, as  $\alpha$  decreases to zero, equations (2 and 3) give the properties of a penny-shaped disc.

### 2.2 Voids formed at inclusions

Figure 2 shows that two types of voids can form at inclusions. One lies completely on the inclusion-matrix interface (Type A), and the other extends into the grain boundary (Type B). Two new angles,  $\beta$  and

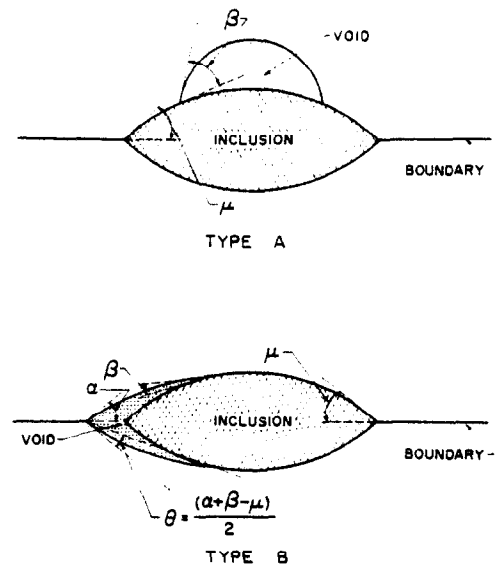


FIG. 2. Two types of voids which can form at inclusions present in a grain boundary.

$\mu$  are needed to describe them. They are shown in Fig. 2 and satisfy the following interface energy relationships:

$$\beta = \cos^{-1} \left\{ \frac{\gamma_{IB} - \gamma_I}{\gamma} \right\} \quad (4)$$

and

$$\mu = \cos^{-1} \left\{ \frac{\gamma_B}{2\gamma_{IB}} \right\}. \quad (5)$$

where  $\gamma_I$  is the energy of the inclusion free surface and  $\gamma_{IB}$  is the energy of the inclusion-matrix interface.

The geometrical properties of the Type A void are given to a good approximation (provided the void is small compared with the inclusion) by equation (2) and the following angle functions:

$$F_V = \frac{\pi}{3} (2 - 3 \cos \beta + \cos^3 \beta) \quad (6a)$$

$$F_S = 2\pi(1 - \cos \beta) \quad (6b)$$

$$F_B = \pi \sin^2 \beta. \quad (6c)$$

The properties of the Type B voids are more difficult to calculate. The exact calculation is given in Appendix I but approximately (to within a factor of two) the volume is given by:

$$V = r^3 \frac{4\pi}{3} \left[ 2 - 3 \cos \left( \frac{\alpha + \beta - \mu}{2} \right) + \cos^3 \left( \frac{\alpha + \beta - \mu}{2} \right) \right]. \quad (7)$$

The reason for this approximation is evident by inspection of Fig. 2.

In the calculations to follow, we shall use the expressions in equations (1-7) and the equations in Appendix I.

### 3. TIME TO FRACTURE: FIXED NUMBER OF NUCLEI

In this section we assume that a fixed number of void nuclei exist, and can grow, as soon as a stress is applied to the hot specimen; and we calculate the time-to-rupture. For this purpose we consider a periodic array of voids in a grain boundary across which a tensile stress  $\sigma_\infty$  is applied. Voids will grow in volume by the diffusion of matter from the void surface into the grain boundary adjacent to the voids as shown in Fig. 3.

Diffusion occurs through the boundary and through the lattice. The steady-state growth of voids by boundary diffusion has been calculated by Hull and Rimmer<sup>(5)</sup> and Speight and Harris.<sup>(4)</sup> Though these solutions are a tolerable approximation for a wide

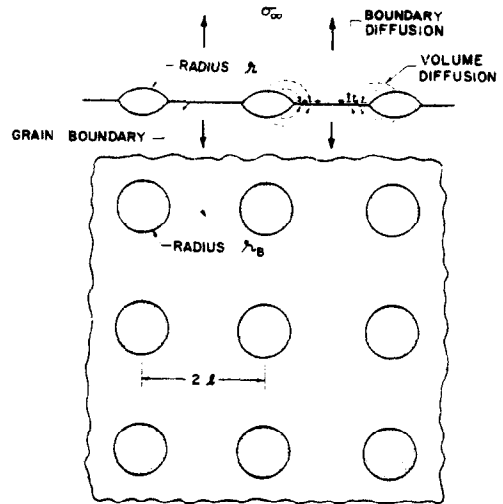


FIG. 3. A periodic array of voids in a grain boundary. A tensile stress of  $\sigma_\infty$  is applied normal to the boundary.

range of void sizes and stresses, they are not strictly correct because they used wrong boundary conditions in solving the diffusion equation.

A calculation that avoids this error is given in Appendix II. The rate-of-growth of the volume of voids which project a circular cross-section of radius  $r_B$  in the grain boundary and are spaced an average distance  $2l$  apart, when growth is by boundary diffusion, is:

$$\left( \frac{dV}{dt} \right)_B = 2\pi\Omega \frac{D_B \delta}{kT} \left( 1 - \frac{r_B^2}{l^2} \right) \times \left[ \frac{\left( \sigma_\infty - \frac{2\gamma}{r} \right) \left( 1 - \frac{r_B^2}{l^2} \right)}{\log_e \left( \frac{l}{r_B} \right) - \frac{3}{4} + \frac{r_B^2}{l^2} \left( 1 - \frac{r_B^2}{4l^2} \right)} \right], \quad (8)$$

where  $r$  is the radius of curvature of the void surface,  $\Omega$  is the atomic volume and  $D_B \delta$  is the boundary diffusion coefficient times the boundary thickness. The equivalent solution for the volume diffusion case is obtained by making the usual approximation:<sup>(6)</sup>

$$\left( \frac{dV}{dt} \right)_{\text{Vol. diff.}} = \left( \frac{dV}{dt} \right)_B \frac{2lD_v}{\pi\delta D_B}. \quad (9)$$

This contribution is added to that given by equation (8) to give the total growth-rate of a void. In practice it is seldom the dominant contribution.

To calculate the time to fracture we define the area-fraction of voids in a grain boundary,  $A(t)$ , as:

$$A(t) = \frac{r_B^2}{l^2}. \quad (10)$$

It is a measure of the damage to the material; that is, extent to which separation has progressed.

Rupture takes place after an elapsed time  $t_r$  when  $A$  reaches a final value  $A_r$ , which we will take to be 0.5. In any real material, holes will nucleate and grow, slowly at first, and then more rapidly as the local load-bearing cross-section is eaten away and the local stress rises. The final fracture must involve the tearing or rapid plastic deformation of the ligaments between the voids; but because hole growth in this final phase is rapid by any mechanism, it occupies only a small part of the life, and we ignore it in calculating  $t_r$ .

The time to fracture,  $t_r$ , has been derived in Appendix II:

$$t_r = \frac{3\sqrt{\pi}}{32} \frac{kT}{\Omega D_B \delta \sigma_\infty \rho^{3/2}} \frac{1}{F_B^{3/2}(\alpha)} \int_{A_{\min}}^{A_{\max}} \frac{dA}{f(A)} \quad (11)$$

where  $\rho$  is the number of voids per unit area of the boundary.

The integral in equation (11) is defined by equation (A2.12). Its value is 0.06 as shown in Fig. A2.1 and as explained in Appendix II. The value of the integral is insensitive to  $A_{\max}$  when  $A_{\max} > 0.1$  and changes very rapidly for  $A_{\max} < 0.1$ , implying that most of  $t_r$  is spent in the early stages of void growth.

The dependence of  $t_r$  on the shape functions  $F_V/F_B^{3/2}$  is shown in Fig. 4. It increases almost linearly with  $\alpha$ . Note that thin penny-shaped voids can be approximated by a small  $\alpha$  while nearly spherical voids by a large  $\alpha$ .

For boundary diffusion  $t_r$  varies as  $1/\rho^{3/2}$ . If the voids were growing by volume diffusion then, in view of equation (9),  $t_r$  would vary as  $1/\rho$ . The time to fracture, normalized with respect to the stress, is plotted in Fig. 5. (The physical constants for copper used in the calculation are given in the Nomenclature:  $\alpha$  was taken to be  $\pi/3$ .) Note that volume diffusion dominates only when void densities are less than

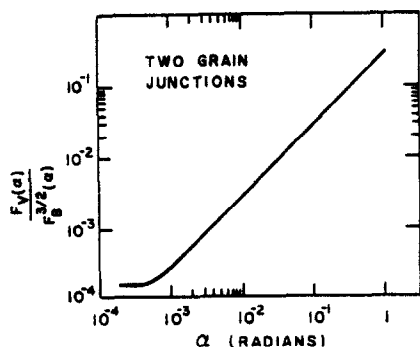


FIG. 4. Dependence of time-to-fracture upon  $\alpha$  for two grain junctions for a fixed number of nuclei.

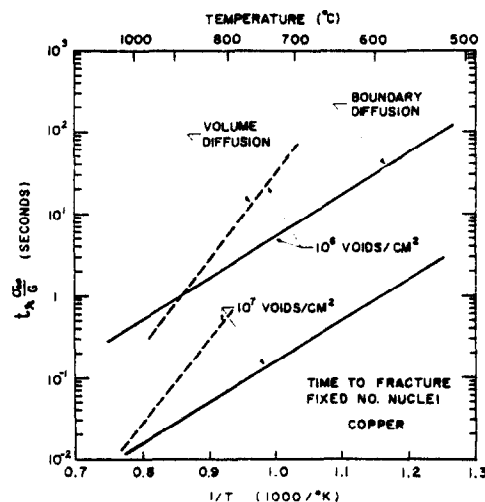


FIG. 5. Variation of time-to-fracture with temperature for a fixed number of nuclei.  $G$  is the shear modulus. The data is for copper (Nomenclature).

$10^6$  voids/cm<sup>2</sup>. Typically, at a stress  $\sigma_\infty = 10^{-4} G$ , at 700°C and for a void density of  $10^6$  voids/cm<sup>2</sup> fracture would occur in one day.

#### 4. NUCLEATION OF VOIDS

In contrast to the last section, we here assume that no voids exist in the virgin specimen, but that they must first be nucleated before they can grow. For this purpose we consider the nucleation of a void in a grain boundary across which a tensile stress  $\sigma_n$  acts. The factors contributing to the change in free energy of the system as a result of forming one void nucleus are: (a) the work done by the system on its surroundings, (b) change in the interface area—and thus energy—within the system and (c) change in the stored elastic energy in the system. Since the term (a) is of order  $\sigma_n$  and the term (c) is of order  $\sigma_n^2/2E$ , and since  $E \gg \sigma_n$ , term (c) may be neglected in comparison with (a). Recalling equations (2) we get the change in free energy:

$$\Delta G = -r^3 F_v(\alpha) \sigma_n + r^2 [\gamma F_S(\alpha) - \gamma_B F_B(\alpha)]. \quad (12)$$

The critical radius,  $r_c$ , at which  $\Delta G$  reaches a maximum, and the magnitude of this maximum,  $\Delta G_c$ , can be calculated using equations (12, 2 and 3) and the equations in Appendix I. The result is a general one and is applicable to all types of void configurations:

$$r_c = \frac{2\gamma}{\sigma_n} \quad (13)$$

and

$$\Delta G_c = \frac{r_c^3 F_v(\alpha) \sigma_n}{2}. \quad (14)$$

Alternatively  $\Delta G_c$  can be written as

$$\Delta G_c = \frac{(\text{Volume of the void of critical size}) \times \sigma_n}{2}. \quad (15)$$

If  $\rho_{\max}$  is the maximum number of potential nucleation sites in the grain boundary per unit area, then the number of critical nuclei per unit area is

$$\rho_c = \rho_{\max} \exp\left(-\frac{\Delta G_c}{kT}\right). \quad (16)$$

The number of supercritical nuclei formed per second is  $\rho_c$  times the time-dependent probability,  $p_t$ , of adding one vacancy to the critical nucleus.  $p_t$  can be derived from the jumping frequency of a vacancy, which is related to the boundary self diffusion coefficient, and from the probability of finding a vacancy at the perimeter of the nucleus of critical size.<sup>(10)†</sup>

$$p_t = \frac{4\pi\gamma}{\sigma_n \Omega} \frac{D_B \delta}{\Omega^{1/3}} \exp(\sigma_n \Omega / kT). \quad (17)$$

Since usually  $\sigma\Omega/kT \ll 1$ , combining equations (13–17) leads to the nucleation rate:

$$\dot{\rho} = \frac{4\pi\gamma}{\Omega^{4/3}\sigma_n} D_B \delta \left(1 + \frac{\sigma_n \Omega}{kT}\right) (\rho_{\max} - \rho) \times \exp\left[-\left(\frac{4\gamma^3 F_v(\alpha)}{\sigma_n^2 kT}\right)\right]. \quad (18)$$

The exponential factor above is the dominant influence in the temperature dependence of nucleation;  $F_v(\alpha)$ ,  $\gamma$  and  $\sigma_n$  are, therefore, the critical parameters in determining the nucleation rate. Note that  $F_v(\alpha) = 0$  if:  $\alpha = 0$  at two grain junctions,  $0 \leq \alpha \leq \pi/6$  at three grain junctions, and  $0 \leq \alpha \leq \sin^{-1}(\frac{1}{2})$  at four grain junctions; at these values of  $\alpha$  there is no kinetic barrier to nucleation. However,  $F_v(\alpha)$  increases rapidly as  $\alpha$  increases beyond these values.

## 5. TIME TO RUPTURE II: CONTINUOUS NUCLEATION, NO GRAIN-BOUNDARY SLIDING

The compound problem of nucleation and growth of voids is solved by combining equation (11) with (18) since  $\rho$ , the void density, now becomes time-dependent. The new equation for  $t_r$  is:

$$0.5 = \frac{32\sqrt{\pi}}{3} \frac{\Omega D_B \delta}{kT} \sigma_n \frac{F_B^3(\alpha)}{F_v(\alpha)} \int_0^{t_r} \int_{\Gamma} \rho^{1/2}(t - \Upsilon) \dot{\rho}(\Upsilon) f(A(t - \Upsilon)) dt d\Upsilon. \quad (19)$$

† This probability is the number of peripheral atom sites  $2\pi r_b \delta \Omega^{1/3} / \Omega$  times the probability  $D_B / \Omega^{2/3}$  that one jumps away from the void. The factor  $e^{\sigma_n \Omega / kT}$  allows for the change in vacancy concentration caused by the stress. In obtaining equation (17), we have approximated  $r_b$  by  $r_c = 2\gamma/\sigma_n$ .

The numerical procedure for solving for  $t_r$  in the above equation is described in Appendix III.

In this section we consider the case where the normal stress in the boundary which causes nucleation,  $\sigma_n$  (equation 18), is equal to the applied stress,  $\sigma_\infty$ ; no stress concentration occurs in the boundary as a result of grain boundary sliding, or as a result of a slip within a grain being obstructed by a boundary.

As an example, consider a copper polycrystal with a grain size of  $10 \mu\text{m}$ , strained at a constant strain-rate of  $10^{-4}/\text{sec}$ . At high temperatures, the polycrystal will flow predominantly by *power-law creep*, or (very close to its melting point) by *diffusional flow*. At lower temperatures its flow is predominantly by the *glide motion of dislocations*. The stress required for flow at a constant rate depends on the way in which the kinetics of the dominant mechanism depend on temperature, and thus varies in a complicated way with temperature. Its behaviour has been described, compared with experiment, and presented in deformation-mechanism diagrams, in earlier publications;<sup>(11,12)</sup> the stress required to maintain a strain-rate of  $10^{-4}/\text{sec}$  in a copper polycrystal was calculated by the method, and using the data, given in these references. The result is shown in Fig. 6. This relationship between stress and temperature has been used to calculate the time-to-rupture for the five possible configurations. These time-to-rupture curves are shown in Figs. 7. All are calculated for a strain-rate of  $10^{-4}/\text{sec}$ , a grain size of  $10 \mu\text{m}$ , and an inclusion density of  $10^{10}/\text{m}^2$ .

The important features of these curves are:

### (a) Ductility minimum

All curves show a minimum time-to-fracture at an intermediate temperature. This is because the rate of fracture is proportional to the product of the nucleation-rate and the growth-rate of the voids. As the

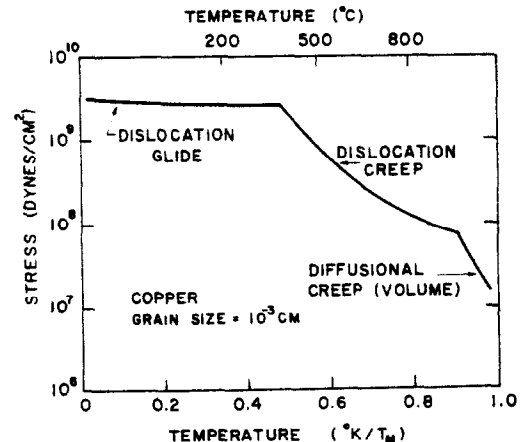


Fig. 6. Variation of stress with temperature when a polycrystal of copper of grain size  $10 \mu\text{m}$  is strained at  $10^{-4}/\text{sec}$ . Data from Refs. 11 and 12.

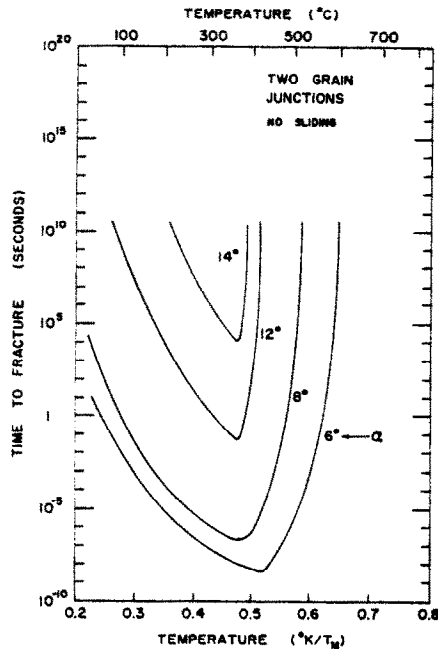


Fig. 7(a). Void nucleation and growth at two grain junctions with no sliding.

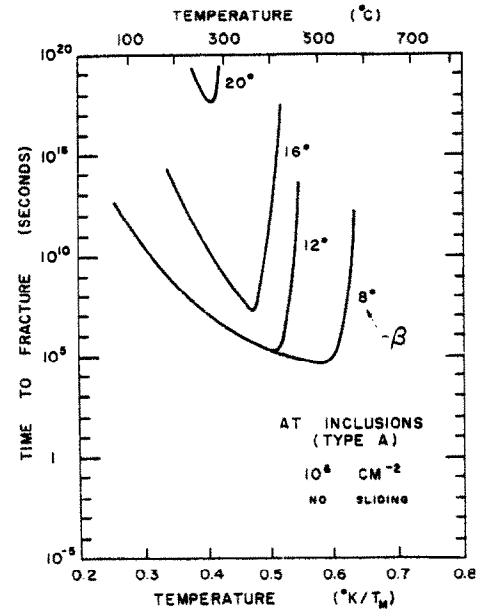


Fig. 7(c). Void nucleation and growth at inclusions for Type A voids with no sliding.

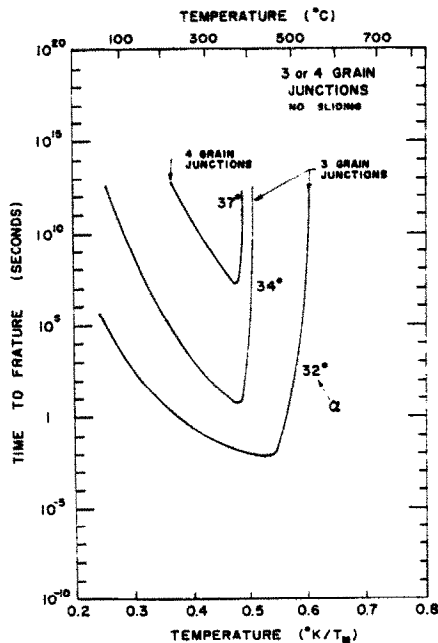


Fig. 7(b). Void nucleation and growth at two, three and four grain junctions with no sliding.

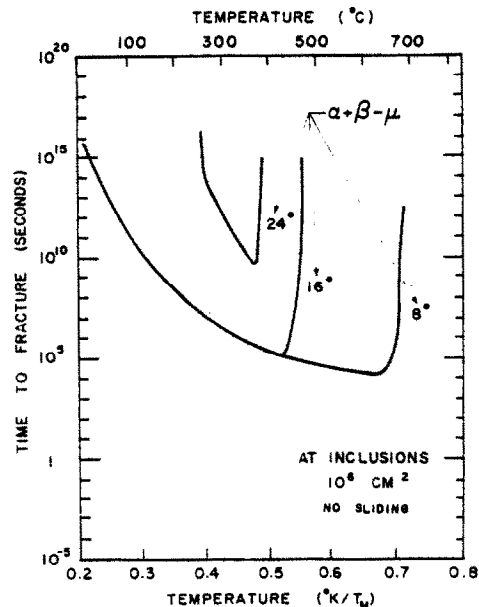


Fig. 7(d). Void nucleation and growth at inclusions for Type B voids with no sliding.

temperature increases, the stress required to maintain a given strain-rate falls in such a way that the growth rate increases, but the nucleation rate decreases. At low temperatures nucleation occurs readily, but the growth rate is small and determines the rupture life, whereas at high temperatures growth is fast and it is the nucleation rate that is small, and determines the

life. This results in a minimum value for  $t_r$  at an intermediate temperature. At temperatures above  $0.7T_M$  nucleation often ceases completely, which precludes intergranular fracture. Note that the minimum moves to a lower temperature as  $\alpha$  increases. The very sharp minimum is partly due to our assumption of a unique, uniform grain-size, and nucleus distribution, so that

all grains cavitate simultaneously and to the same extent. Any spread in these quantities broadens the minimum.

(b) *Nucleation rate*

When no grain boundary sliding is allowed, as in the present case, then, in general, nucleation is continuous with time i.e., the number of nuclei increases with time towards the number  $\rho_{max}$ .

(c) *Sensitivity to  $\alpha$*

$\alpha$  by its definition in equation (1) is the primary measure of the surface energy barrier to void nucleation. At two-grain junctions, for instance, the energy barrier to nucleation vanishes as  $\alpha$  goes to zero, but grows, causing the nucleation rate to decrease rapidly, as  $\alpha$  increases from 6 to 14° (Fig. 7a). For three- and four-grain junctions there is no barrier to nucleation when  $\alpha = 30$  and 36° respectively. A slight increase in  $\alpha$  above these limits causes a rapid change in nucleation rate as shown in Fig. 7(b) nucleation ceases when  $\alpha = 37^\circ$ . Since for a pure metal,  $\alpha \approx 75^\circ$ , no nucleation will occur unless inclusions are present in the boundaries.

(d) *Type A and type B voids*

For Type A voids at inclusions the angle  $\beta$  (Fig. 2) is the important surface energy parameter. Fracture is possible for  $\beta < 20^\circ$  as shown in Fig. 7(c). The parameter  $(\alpha + \beta - \mu)$  as described in Fig. 2 and Section 1 is a measure of the surface energy barrier for Type B voids forming at inclusions. As shown in Fig. 7(d) fracture is possible if  $(\alpha + \beta - \mu) < 24^\circ$ . In general, Type B nucleation sites will be favored when  $\mu < \alpha$ , i.e. when  $\gamma_{IB} < \gamma$  (by consideration of equations (1 and 5)).

6. TIME TO RUPTURE III: CONTINUOUS NUCLEATION, WITH SLIDING

6.1 *Stress concentration at inclusions due to sliding*

Sliding across an inclusion in a grain boundary must be accommodated.<sup>(9,13)</sup> If the sliding displacements are too large to be accommodated elastically, then accommodation must be by diffusional flow or plastic flow (Fig. 8). The upper bound for the steady-state

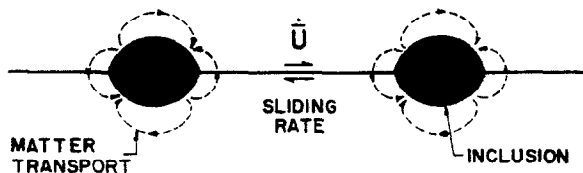


FIG. 8. Sliding across an inclusion must be accommodated by transport of matter.

stress<sup>†</sup> that can be maintained at an inclusion during creep is that required to drive the diffusive fluxes, either by lattice or by boundary diffusion, which will accommodate the incompatibility which appears there. Following a procedure described earlier<sup>(9)</sup> the normal traction at the interface,  $\sigma_n$ , can be calculated for an imposed sliding rate  $\dot{U}$  at the boundary; typically its magnitude is (Ref. 9, Appendix B)

$$\sigma_n = \frac{kT}{1.6\Omega} \frac{p\dot{U}}{D_v \left( 1 + \frac{5\delta D_B}{pD_v} \right)}, \quad (20)$$

where  $p$  is the diameter of an inclusion. For a strain rate of  $\dot{\epsilon}$  and a grain size of  $d$ , the maximum possible sliding rate is

$$\dot{U} = \dot{\epsilon}d \quad (21)$$

Substituting this into equation (20) gives the upper bound for  $\sigma_n$ .

The time to fracture curves shown in Figs. 9(a and b) were evaluated by using this estimate of  $\sigma_n$  in equation (18 and 19).

6.2 *Fracture curves for type A and type B voids*

Fracture curves for Type A are given in Fig. 9(a) and for Type B voids in Fig. 9(b). Fracture is now possible

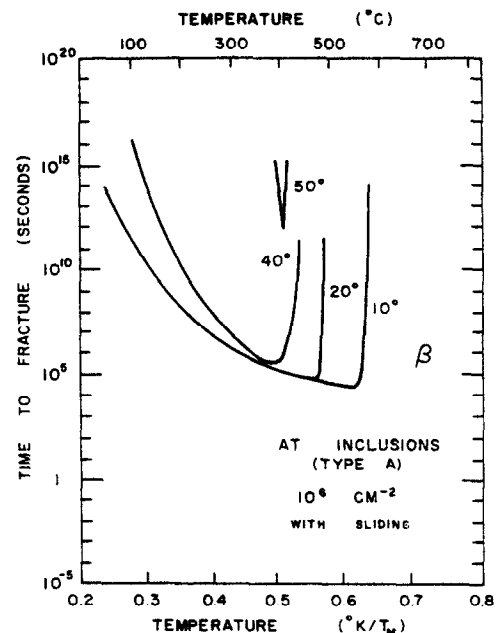


FIG. 9(a). Void nucleation and growth at inclusion for Type A voids with sliding.

† On initial loading, or when the stress is suddenly changed, much larger stresses can appear:<sup>(21)</sup> these relax to the value quoted above with a characteristic relaxation time; but during that time, nucleation may occur.

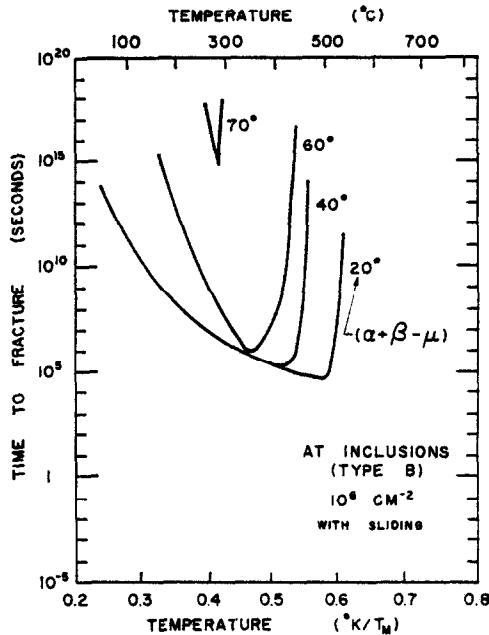


Fig. 9(b). Void nucleation and growth at inclusion for Type B voids with sliding.

for  $\beta < 40^\circ$  and for  $(\alpha + \beta - \mu) < 70^\circ$ . It becomes easier to nucleate Type B voids than Type A voids. The ductility minimum is observed in these curves for the same reasons as before; and, as before, the minimum moves to a lower temperature as the energy angle is increased. The nucleation behaviour, however, is different: instead of continuous nucleation we now get catastrophic nucleation: full nucleation occurs early in the fracture process. There are two reasons for this: first the maximum number of nucleation sites (equal to the number of inclusions) is fewer; and second,  $\sigma_n$  varies more rapidly with temperature than  $\sigma_\infty$  (at a constant strain-rate).

The value of the parameters used in the generation of Figs. 9(a and b) were: inclusion size  $1 \mu\text{m}$ , grain size  $10 \mu\text{m}$ , inclusion density  $10^{10}/\text{m}^2$ , and strain-rate  $10^{-4}/\text{sec}$ .

### 6.3 Sensitivity of fracture curves to different parameters

Figures 10–14 demonstrate the sensitivity of the fracture curves to strain rate, grain size, particle size, particle density and the distribution of particles. All curves were plotted for  $\alpha + \beta - \mu = 40^\circ$  (except in Fig. 10 where  $\alpha + \beta - \mu = 20^\circ$ ) and for  $\alpha = 35^\circ$ , and (except where otherwise noted) a strain-rate of  $10^{-4}/\text{sec}$ , a grain size of  $10 \mu\text{m}$ , an inclusion density of  $10^{10}/\text{m}^2$  and an inclusion size of  $1 \mu\text{m}$ . Stress concentration due to sliding was taken into account and Type B void nucleation was considered. The relative

aspects of the results would have remained the same if a different set of conditions had been chosen.

(i) *Strain-rate* (Fig. 10). As strain rate decreases the minimum moves to a lower temperature and to a higher value for time-to-fracture. For example, at a strain rate of  $10^{-4}/\text{sec}$  the minimum occurs at  $0.58 T_M$  and the time-to-fracture is  $4.3 \times 10^4 \text{ sec}$ ; at  $10^{-6} \text{ sec}$  the values are  $0.44 T_M$  and  $1.6 \times 10^6 \text{ sec}$ .

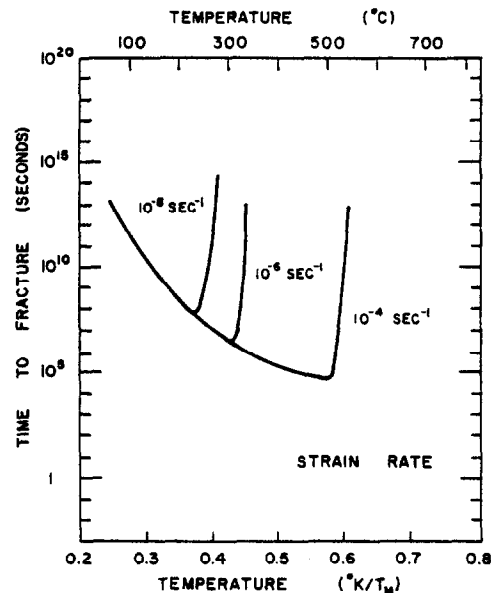


Fig. 10. The influence of strain rate on ductility.  $\alpha + \beta - \mu = 20^\circ$ , Type B voids.

(ii) *Grain size* (Fig. 11). A smaller grain size improves ductility; it moves the minimum to a lower temperature and a higher value of time-to-fracture. For example, for a grain size of  $10 \mu\text{m}$  the minimum occurs at  $0.52 T_M$  and the time-to-fracture is  $1.2 \times 10^5 \text{ sec}$  whereas for a grain size of  $100 \mu\text{m}$  the values are  $0.62 T_M$  and  $2.4 \times 10^4 \text{ sec}$ . These conclusions are in qualitative agreement with published experimental work.<sup>(14,15)</sup>

(iii) *Inclusion size* (Fig. 12). A smaller particle size improves ductility. For example for a particle size of  $1 \mu\text{m}$  the minimum occurs at  $0.52 T_M$  and the time-to-fracture is  $1.2 \times 10^5 \text{ sec}$  whereas for a particle size of  $0.1 \mu\text{m}$  the values are  $0.4 T_M$  and  $1.2 \times 10^7 \text{ sec}$ .

(iv) *Inclusion density* (Fig. 13). As expected from equation (11) the time-to-rupture varies inversely as the three-halves power of the number of inclusions per unit area in the grain boundary.

(v) *Distribution of the second phase* (Fig. 14). Fracture curves are shown when the distribution of the second phase in the grain boundary changes although its total volume fraction remains constant. A larger

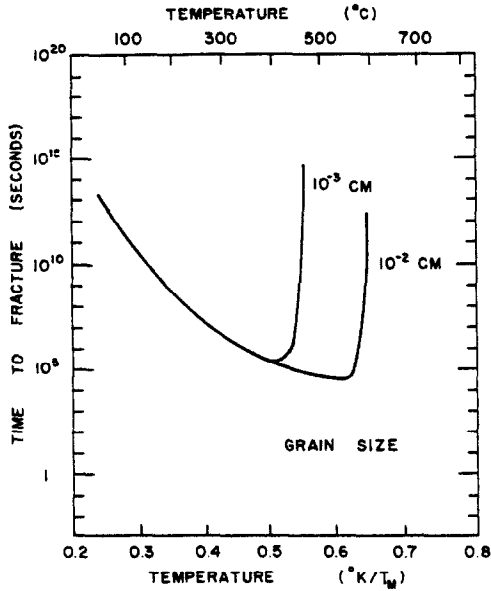


FIG. 11. The influence of grain size on ductility. Type B voids.

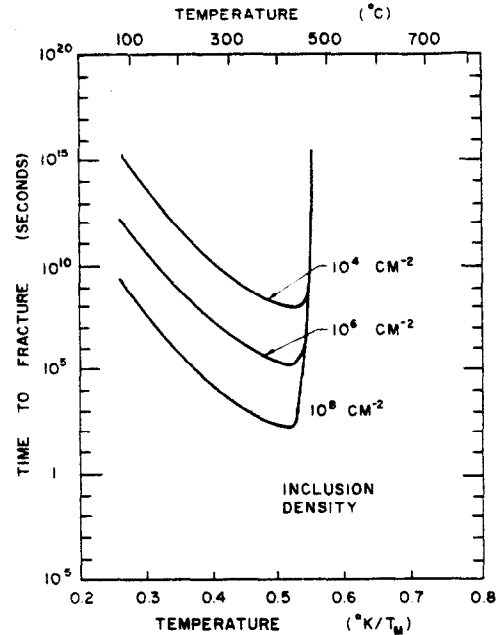


FIG. 13. The influence of inclusion density on ductility.  $\rho = 10^{-6}$  m. Type B voids.

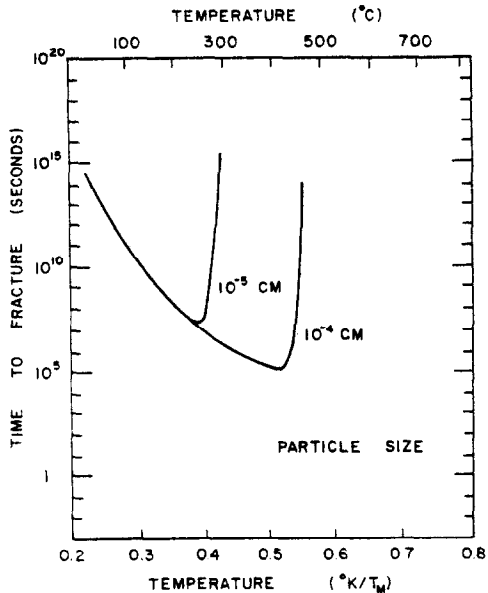


FIG. 12. The influence of inclusion size on ductility. Type B voids.

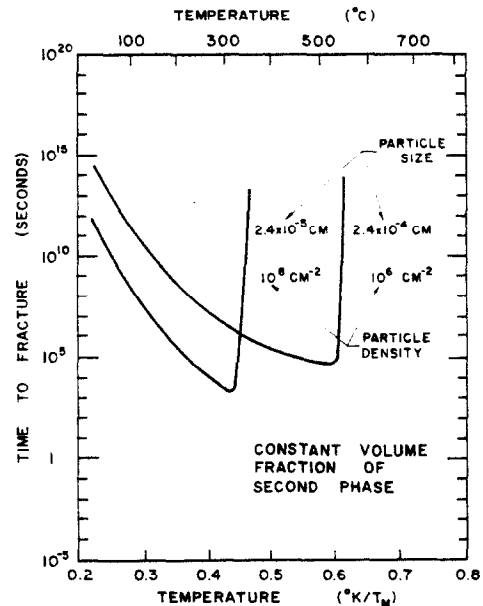


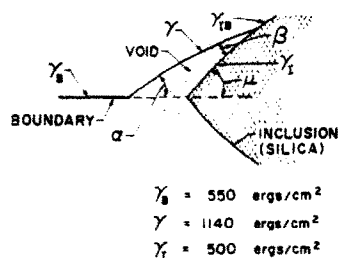
FIG. 14. The influence of the dispersion of second with the total volume of the second phase remaining constant. Type B voids.

particle size moves the minimum to a higher temperature but also raises it to a higher value of time-to-fracture. For large particles the minimum occurs at  $0.6T_M$  and  $3.4 \times 10^4$  sec while for the small particles it occurs at  $0.44T_M$  and  $1.6 \times 10^3$  sec.

#### 6.4 The role of interface energies

It has been shown that the nucleation of voids is sensitive to the energy angle  $\beta$  for Type A voids and to

$(\alpha + \beta - \mu)$  for Type B voids. The dependence of these angles on interface energies has been described in Section 2. Four interfacial energies are involved:  $\gamma$  and  $\gamma_I$ , the matrix free surface and the inclusion free surface energy; and  $\gamma_B$  and  $\gamma_{IB}$ , the grain boundary interface and the inclusion-matrix interface energy. As an example, consider the case of grain boundaries in copper containing silica inclusions. The interface energies are approximately:  $\gamma = 1.14 \text{ J/m}^2$ ,  $\gamma_I = 0.5 \text{ J/m}^2$ ,  $\gamma_B = 0.55 \text{ J/m}^2$ .<sup>(16)</sup> The angles  $\alpha$ ,  $\beta$  and  $\mu$



$\gamma_{IB}$ ergs/cm <sup>2</sup>	$\alpha^\circ$	$\beta^\circ$	$\mu^\circ$	$(\alpha - \beta - \mu)^\circ$
500	76	90	56	110
1000	76	64	74	66
1070	76	60	76	60
1250	76	48	77	47
1370	76	40	78	38
1500	76	28	80	24

TYPE A VOIDS (for  $\beta < 40^\circ$ )  
 TYPE B VOIDS (for  $\alpha + \beta - \mu < 60^\circ$ )

FIG. 15. The angle and interface energy relationship for a copper polycrystal containing silica inclusions. Void nucleation is possible for  $\beta < 40^\circ$  (Type A voids) and for  $\alpha + \beta - \mu < 60^\circ$  (Type B voids).

are given in Fig. 15 for various values of  $\gamma_{IB}$ . From consideration of results in this section we conclude that nucleation of Type A voids is possible for  $\beta < 40^\circ$  or for  $\gamma_{IB} < 1.37 \text{ J/m}^2$ . Nucleation of Type B voids is possible for  $(\alpha + \beta - \mu) < 60^\circ$  or for  $\gamma_{IB} < 1.07 \text{ J/m}^2$ . These limits are good only for the set of creep conditions specified in this paper. The limits for other cases can be calculated.

## 7. SUMMARY AND DISCUSSION

The kinetics of stress induced nucleation and growth voids in a grain boundary has been analysed in detail. Particular attention has been given to voids forming at second phase particles since these appear to be the prime sites for nucleation in the grain boundary. The cogent results are:

(a) Three types of void configuration in clean boundaries and two types of configurations at second phase particles are possible. The geometrical properties of all the configurations can be described by similar general functions. General solutions for the nucleation and growth of these voids are therefore possible.

(b) An expression for time-to-fracture has been derived for growth by boundary diffusion when the number of voids remains constant. The results are extrapolated to include growth by volume diffusion. The early stage of void growth is the slowest and accounts for most of the time-to-fracture.

(c) Using classical nucleation theory, the nucleation of the voids has been calculated. The energy barrier

for nucleation is a sensitive function of the free surface energy and of the volume of the void of critical radius.

(d) A numerical procedure has been developed which gives the time-to-fracture when nucleation and growth occur continuously and simultaneously.

(e) The time-to-rupture curves have been obtained for the case when a polycrystal is deformed at a constant strain-rate at different temperatures. When no sliding of the boundaries is allowed then void nucleation is possible only when interface energies are comparable to the total surface energy of the void being created. These conditions may be met at non-wetting or almost non-wetting inclusions.

(f) Stress concentrations are produced when sliding occurs in a boundary which contains inclusions. Upper bounds for these stresses are calculated and new time-to-fracture curves are obtained. Inclusions now become probable nucleation sites. Quantitative results are derived in terms of all the surface energies involved in the nucleation process.

(g) The time-to-fracture vs temperature curves show a minimum ductility at approximately  $0.5T_M$ . This is in agreement with the published experimental work.<sup>(2,3,17)</sup>

(h) The time-to-fracture curves shift with change in strain-rate, grain size, inclusion size, inclusion density and the distribution of the second phase. For results see Figs. 10-14.

(i) When no sliding is allowed the number of nuclei increase continuously with time but when stress concentrations due to sliding are taken into account then nucleation is catastrophic i.e. full nucleation occurs in the early stages of creep. Experimental work in support of the first<sup>(1,18)</sup> as well as the second process<sup>(6,19)</sup> is found in the literature.

(j) The results are applied to a copper polycrystal of grain size  $10 \mu\text{m}$  being strained at  $10^{-4}$  sec and containing silica inclusion of size  $1 \mu\text{m}$  dispersed at a density of  $10^{10}/\text{m}^2$  in the boundaries.

## ACKNOWLEDGEMENTS

This work was supported by a grant from the Air Force Office of Scientific Research, No. 73-2501. We gratefully acknowledge helpful discussions with Professor D. Turnbull and Dr. H. J. Frost, and the critical comments of Dr. P. G. Shewmon. We wish to acknowledge a grant from the Kennecott Copper Corporation which made part of this work possible.

## REFERENCES

1. R. T. RATCLIFFE and G. W. GREENWOOD, *Phil. Mag.* **12**, 59 (1965).
2. G. D. BENGOUGH, *J. Inst. Met.* **7**, 123 (1912).
3. F. N. RHINES and P. J. WRAY, *Trans. ASM* **54**, 117 (1961).

4. M. V. SPEIGHT and J. E. HARRIS, *Met. Sci. J.* **1**, 83 (1967).
5. D. HULL and D. E. RIMMER, *Phil. Mag.* **4**, 673 (1959).
6. P. R. OLIVER and L. A. GIRIFALCO, *Acta Met.* **10**, 765 (1962).
7. J. E. HARRIS, *Trans. Met. AIME* **233**, 1509 (1965).
8. P. J. CLEMM and J. C. FISHER, *Acta Met.* **3**, 70 (1955).
9. R. RAJ and M. F. ASHBY, *Trans. Met. AIME* **2**, 1113 (1971).
10. P. G. SHEWMON, *Diffusion in Solids*, Chapter 2. McGraw-Hill, New York (1963).
11. M. F. ASHBY, *Acta Met.* **20**, 887 (1972). *Microstructure and design of alloys. Proc. 3rd Int. Conf. Strength of Metals and Alloys*. Vol. 2, p. 8 (1973).
12. H. J. FROST and M. F. ASHBY, Harvard University Rept. A second report on deformation mechanism maps (August 1973).
13. R. RAJ and M. F. ASHBY, *Trans. Met. AIME* **3**, 1937 (1972).
14. D. M. R. TAPLIN and V. N. WHITTAKER, *J. Inst. Met.* **92**, 426 (1963-64); P. K. VENKITERSWARAN, D. C. FERGUSON and D. M. R. TAPLIN, Presented at Met. Soc. of AIME Fall Meeting at Detroit, Michigan, (October 1971).
15. G. J. COCKS and D. M. R. TAPLIN, *Scripta Met.* **3**, 623 (1969).
16. W. T. READ, *Dislocations in Crystals*, Chapter 13. McGraw-Hill, New York (1953).
17. B. J. REID and J. N. GREENWOOD, *Trans. Met. AIME* **12**, 503 (1958).
18. G. W. GREENWOOD, *Phil. Mag.* **19**, 423 (1969).
19. H. E. EVANS and J. S. WADDINGTON, *Phil. Mag.* 1075 (1969).
20. C. HERRING, *J. appl. Phys.* **21**, 437 (1950).
21. R. RAJ. To appear in *Met. Trans.* (1975).

NOMENCLATURE

$\gamma$	surface free energy per unit area of the matrix material
$\gamma_B$	interface free energy per unit area of the matrix grain boundary
$\gamma_I$	surface free energy of the inclusion
$\gamma_{IB}$	interface free energy of the inclusion-matrix boundary
$V$	total volume of the void
$S$	total surface area of the void
$B$	area of the grain boundary which the void occupies
$F_v$	a function of energy angles which provides the void volume (equation 3a)
$F_S$	a function of energy angles which provides the void surface area (equation 3c)
$F_B$	a function of energy angles which provides the area $B$ (equation 3c)
$\alpha$	energy angle as defined by equation (1)
$\beta$	energy angle as defined by equation (4) (also a constant in the calculation of appendix II)
$\mu$	energy angle as defined by equation (5)
$D_B$	grain boundary self-diffusion coefficient—its value for copper: $10^{-5} \exp(-24.8 \text{ kcal/mole}/RT) \text{ m}^2/\text{sec}$
$D_v$	lattice self-diffusion coefficient—its value for copper: $6.2 \times 10^{-5} \exp(-49.6 \text{ kcal/mole}/RT) \text{ m}^2/\text{sec}$
$\delta$	boundary thickness—its value: $4 \times 10^{-10} \text{ m}$

$r$	radius of curvature of the void surface
$r_B$	radius of curvature of the projection of the void in the grain boundary
$2l$	average spacing between the voids
$A$	a fractional measure of the grain boundary area occupied by voids, defined by equation (10)
$\Omega$	atomic volume—for copper: $1.1 \times 10^{-29} \text{ m}^3$
$\sigma_\infty$	external applied stress
$\sigma_n$	local normal stress at the interface which is responsible for void nucleation
$E$	Young's modulus—for copper: $12.7 \times 10^4 \text{ MN/m}^2$
$G$	shear modulus—for copper: $4.2 \times 10^4 \text{ MN/m}^2$
$r_c$	critical radius for void nucleation
$\Delta G_c$	free energy barrier to void nucleation
$\rho$	void density of the number of voids per unit area in the grain boundary
$\rho_{\max}$	maximum number of possible nucleation sites per unit area
$\rho_c$	number of critical nuclei per unit area
$\rho_p$	number of inclusions per unit area of boundary
$p_t$	time dependent probability of adding one vacancy to a nucleus of critical size
$\rho$	nucleation rate of voids per unit area
$t_r$	time to fracture in sec
$\epsilon$	strain rate
$d$	grain size
$\bar{C}$	average sliding rate of a grain boundary
$p$	diameter of the inclusion
$T_n$	normal tractions in the grain boundary which cause growth
$\Delta\mu$	the excess chemical potential of the atoms in the boundary relative to the stress free state
$J_B$	boundary flux of atoms
$\beta$	net number of atoms leaving per unit volume of the grain boundary during the steady state growth of voids.

APPENDIX I

(a) *Properties of voids in inclusion free boundaries*

The  $F(\alpha)$  functions in equation (2) for the three and four grain junctions are as follows (8).

*Three grain junctions*

$$F_v(\alpha) = 2 \left[ \pi - 2 \sin^{-1} \left( \frac{1}{2} \csc \alpha \right) + \frac{1}{3} \cos^2 \alpha (4 \sin^2 \alpha - 1)^{1/2} - \cos^{-1} \left( \frac{\cot \alpha}{\sqrt{3}} \right) \cos \alpha (3 - \cos^2 \alpha) \right] \quad (\text{A1.1})$$

and

$$F_s(\alpha) - 2 \cos \alpha F_B(\alpha) = 3F_v(\alpha). \quad (\text{A1.2})$$

## Four grain junctions

$$F_v(x) = 8 \left[ \frac{\pi}{3} - \cos^{-1} \frac{\sqrt{2} - \cos \alpha \cdot (3 - A^2)^{1/2}}{A \sin \alpha} \right] \\ + A \cos \alpha [(4 \sin^2 \alpha - A^2)^{1/2} - A^2/\sqrt{2}] \\ - 4 \cos \alpha (3 - \cos^2 \alpha) \sin^{-1} \left( \frac{A}{2 \sin \alpha} \right),$$

where

$$A = \frac{2}{3} [\sqrt{2}(4 \sin^2 \alpha - 1)^{1/2} - \cos \alpha], \quad (\text{A1.3})$$

and where equation (A1.2) still connects the different  $F$  functions.

## (b) Exact expression for volume of a type B void

The volume of the region shown in Fig. A1 is given by the following expression:

$$V = 2r^3(I_1 + I_2),$$

where

$$I_1 = \int_{\sin(\mu-\alpha)}^L \left\{ (1-x^2) \cos^{-1} \frac{Z}{\sqrt{1-x^2}} \right. \\ \left. - Z\sqrt{1-x^2-z^2} \right\} dx,$$

and

$$I_2 = \int_L^{\sin \beta} (1-x^2) \cos^{-1} \frac{\beta}{\sqrt{1-x^2}} \\ - \cos \beta \sqrt{\sin^2 \beta - x^2} \Big\} dx, \quad (\text{A1.4})$$

where

$$L = \frac{\cos \alpha - \cos \beta \cos \mu}{\sin \mu}$$

and

$$Z = \frac{\cos \alpha - x \sin \mu}{\cos \mu}.$$

The integral was evaluated numerically.

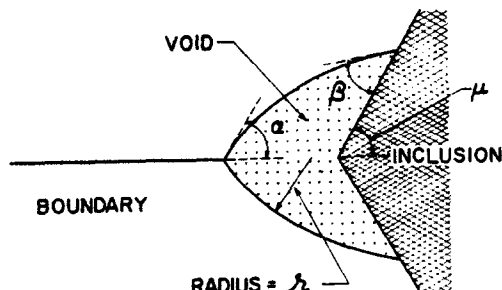


FIG. A1. Evaluation of volume of a Type B void.

## APPENDIX II

## Time-to-Fracture: Fixed Number of Nuclei

## (a) Steady state void growth rate

Let  $T_n(R)$  be the normal tractions in the grain boundary in Fig. 3. The excess chemical potential of atoms in the boundary relative to the stress free state is<sup>(20)</sup>

$$\Delta\mu = -T_n\Omega. \quad (\text{A2.1})$$

The transport equation for boundary diffusion is:

$$\mathbf{J}_B = -\frac{D_B}{\Omega kT} \nabla(\Delta\mu) \quad (\text{A2.2})$$

The steady-state condition is that all parts of the boundary must give up or add the same amount of material, i.e.

$$\nabla \cdot \mathbf{J}_B = \beta, \quad (\text{A2.3})$$

where  $\beta$  is a constant and is equal to the number of atoms removed per unit volume of the boundary which is thought of as having a thickness  $\delta$ . These equations lead to the differential equation

$$\nabla^2(\Delta\mu) = -\frac{\beta kT\Omega}{D_B} \quad (\text{A2.4})$$

which must be solved (in polar coordinates with circular symmetry) subject to the boundary conditions:

$$\frac{\partial \Delta\mu}{\partial R} = 0, \quad \text{at } R = l, \quad (\text{A2.5a})$$

and

$$\Delta\mu = -\frac{2\gamma\Omega}{r}, \quad \text{at } R = r_B. \quad (\text{A2.5b})$$

The answer is:

$$\Delta\mu = -\frac{\beta kT\Omega}{4D_B} (R^2 - r_B^2) \\ - \frac{\beta kT\Omega l^2}{2D_B} \log_e \frac{r_B}{R} - \frac{2\gamma\Omega}{r}. \quad (\text{A2.6})$$

The condition of mechanical equilibrium requires that:

$$\pi l^2 \sigma_\infty = \int_{r_B}^l T_n(R) 2\pi R dR. \quad (\text{A2.7})$$

Substituting equations (A2.1 and A2.6) in (A2.7) gives an expression for  $\beta$ . Since the growth rate of the void is equal to the amount of material added in the grain boundary, we have:

$$\frac{dV}{dt} = -\beta \delta \pi l^2 \Omega \left( 1 - \frac{r_B^3}{l^3} \right). \quad (\text{A2.8})$$

Substitution of  $\beta$  leads to the final result given in equation (8).

## (b) Calculation of time-to-fracture

Using the definition for  $A(t)$  given in equation (10) and recalling from equations (2) that

$$r_B^2 = \frac{r^2}{\pi} F_B(\alpha) \quad (\text{A2.9a})$$

and

$$V = r^3 F_V(\alpha), \quad (\text{A2.10a})$$

equation (8) can be re-written in the following form:

$$\frac{dA}{dt} = \frac{32}{3\sqrt{\pi}} \frac{\Omega D_B \delta}{kT} \sigma_x \rho^{3/2} \frac{F_B^{3/2}(\alpha)}{F_V(\alpha)} f(A). \quad (\text{A2.11})$$

where

$$f(A) = \frac{(1-A)}{\sqrt{A}} \times \frac{\{1 - (r_c/r)(1-A)\}}{\frac{1}{2} \log_e 1/A - \frac{3}{4} + A(1-A/4)}. \quad (\text{A2.12})$$

Here  $r_c$  is the critical radius given by:

$$r_c = \frac{2\gamma}{\sigma_x} \quad (\text{A2.13})$$

and  $\rho$  is the number of voids per unit area of the boundary:  $\rho = 1/(2l)^2$ . Equation (A2.11) leads to an expression for time to fracture,  $t_r$ :

$$t_r = \frac{3\sqrt{\pi}}{32} \frac{kT}{\Omega D_B \delta} \frac{1}{\sigma_x \rho^{3/2}} \frac{F_V(\alpha)}{F_B^{3/2}(\alpha)} \int_{A_{\min}}^{A_{\max}} \frac{dA}{f(A)}. \quad (\text{A2.14})$$

The integral in equation (A2.14) has been evaluated where the voids start to grow from critical size (A2.13). Its value, for  $r_c = 100 \text{ \AA}$ , and for a variable upper limit, is shown in Fig. A2. It is evident that the early stages of void growth are the slowest. The integral becomes relatively insensitive to  $A_{\max}$  after  $A_{\max} > 0.1$ . In all computations in this paper we assume  $A_{\max} = 0.5$  for which the integral is equal to 0.06.

The integral is also insensitive to the value of  $A_{\min}$ , defined by:

$$A_{\min} = \frac{r^2 F_B(\alpha) \rho}{\pi}. \quad (\text{A2.15})$$

This can be seen from Fig. A2, in which a variation of  $\rho$  (and thus of  $A_{\min}$ ) by a factor of  $10^8$  makes little difference to the value of the integral.

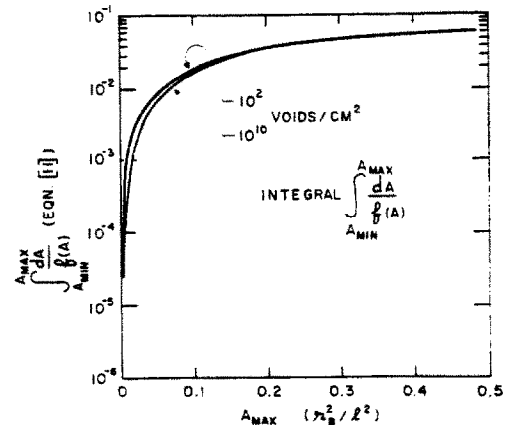


FIG. A2. The change in time-to-fracture (the integral is proportional to it) with  $\alpha$  for two grain junctions.

## APPENDIX III

## Nucleation and Growth of Voids: A Computer Model

A computer model was developed to simulate the continuous nucleation and growth of voids in the grain boundary. Simultaneous nucleation and growth was assumed to occur at a constant rate during small, but discrete, time intervals  $\Delta t_x$  where the subscript determines the sequence of the time intervals. The radius of a void,  $r_{ij}$ , in the  $j$ th period depends upon the  $i$ th period during which it was born. The number of nuclei of radius  $r_{ij}$ ,  $\Delta \rho_i$  will be given by:

$$\Delta \rho_i = \dot{\rho}_i \Delta t_i \quad (\text{A3.1})$$

where  $\dot{\rho}_i$  is given by equation (18). When all the nucleation sites,  $\rho_{\max}$ , have been exhausted, the nucleation rate goes to zero. New nuclei are assigned the critical radius (equation A2.13).

The computer simulation operates using equations (8 and 2). At every time step the fractional grain boundary interface which has been replaced by voids is calculated according to:

$$A_j = \Delta \rho_i r_{ij}^2 F_B(\alpha). \quad (\text{A3.2})$$

The value of  $j$ , for which  $A_j \geq 0.5$ , is determined and the time to fracture is then equal to  $\sum_{k=1}^j \Delta t_k$ . If the value of  $j$  is less than 25,  $\Delta t$  is decreased until  $j > 25$ . Increasing the minimum value of 'j' from 25 to 50 increased the accuracy by only 10 per cent whereas the computer time needed for the calculation increased logarithmically.

At two-, three- and four-grain junctions,  $\rho_{\max}$  was set equal to

$$\frac{1}{(\bar{r}_c^2 F_B(\alpha))}; \quad \frac{1}{(\bar{r}_c dF_B^{1/2}(\alpha))}; \quad \text{and} \quad \frac{2}{d^2}$$

respectively. Here  $d$  is the grain size, and  $\bar{r}_c$  is the radius of a nucleus equal to the volume sum of the critical nucleus plus one atomic volume.

$\rho_{\max}$  was taken to be equal to  $(p^2\rho_p/b^2)$  when inclusions were present,  $p$  is the inclusion size and  $\rho_p$  the inclusion density in the grain boundary. However,

for inclusions, all the nucleation sites were considered to be exhausted when the total number of nuclei was equal to the number of inclusions. The stress in equation (18) was assigned an upperbound value of  $2.0 \times 10^3$  MN/m<sup>2</sup> which was assumed to be the ideal fracture strength of the interface.